ACS OMEGA

Open Access

http://pubs.acs.org/journal/acsodf

Article

PdRu Bimetallic Nanoparticles/Metal−Organic Framework Composite through Supercritical CO_2−Assisted Immobilization

Kiyoshi Matsuyama,* Takumi Matsuoka, Masashi Eiro, Takafumi Kato, and Tetsuya Okuyama

Cite This: *ACS Omega* 2024, 9, 20437−20443

Read Online

ACCESS | Metrics & More | Article Recommendations | Supporting Information

ABSTRACT: Metal−nanoparticle (NP)/metal−organic framework (MOF) composites have attracted considerable attention as heterogeneous catalysts. Compared with porous carbon, silica, and alumina, the charge-transfer interaction between the metal NPs and the MOF accelerated the catalytic activity. In this study, PdRu bimetallic NPs were successfully immobilized on MOFs such as MIL-101(Cr) by using supercritical carbon dioxide. The STEM-EDX images show a uniform 3D distribution of the PdRu bimetallic NPs on MIL-101(Cr). The resulting PdRu@MIL-101(Cr) catalyst exhibited higher CO oxidation than monometal/MOF composites such as Pd@MIL-101(Cr) and Ru@MIL-101(Cr). Furthermore, PdRu@MIL-101(Cr) exhibited higher catalytic activity than PdRu@SiO_2. This is because the particle size of the PdRu bimetallic NPs in MIL-101(Cr) was within the range of 2−3 nm. The synergistic effects were based on the combination of two metals, Pd and Ru, small bimetal particle formation, and charge-transfer interactions between the bimetal NPs and the MOF. These factors enhance the catalytic activity of the bimetal/MOF composites.

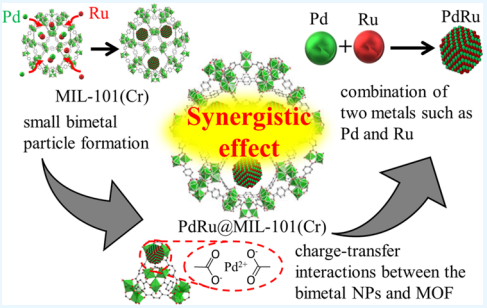

1. INTRODUCTION

Metal−organic frameworks (MOFs), also known as porous coordination polymers (PCPs), have recently gained recognition as crystalline nanoporous materials. These materials have potential applications such as gas storage,[1] separation of compounds from mixture,[2] biomedicine,[3] and catalysis.[4,5] Metal nanoparticles (NPs) immobilized on the pores and surfaces of MOFs (NP@MOFs) have attracted significant attention as useful heterogeneous catalysis materials.[6,7] MOFs are promising catalytic supports for metal NPs, and the deposition of metal NPs onto MOFs enhances their catalytic performance. MOFs have porous structures and large specific surface areas that allow the loading of highly dispersed metal NPs, effectively preventing agglomeration and leaching. Furthermore, the synergistic effects of metal NPs and MOFs have attracted significant interest in intelligent heterogeneous catalysis. Metal NP/MOF composites have the potential to exhibit specific support effects such as molecular sieving, charge transfer, and selective substrate adsorption in heterogeneous catalysis.[8] MOFs are promising candidates for replacing traditional porous support materials with metal NPs, such as inorganic silica, alumina, and carbon materials. MOFs facilitate the control of catalytic activity when used as supports for metal NPs in heterogeneous catalysis. This occurs because of the electronic interactions between the MOFs and metal NPs.[8,9]

Bimetallic NPs consist of two metals and have attracted widespread attention because their structure and properties often differ from those of their monometallic analogs.[10−12] The structure and combination of the two active metals may provide a synergistic effect when bimetallic NPs are used as catalysts. In general, the catalytic properties of bimetallic NPs are superior to those of their monometallic counterparts. In the field of heterogeneous catalysis, combinations of bimetallic NPs and MOFs have recently attracted considerable attention.[13] The catalysis of CO oxidation using bimetallic NPs supported on MOFs was significantly higher than that using any of the reported monometallic NPs supported on MOFs.[14,15] The combination of bimetallic NPs with MOFs is considered one of the most effective strategies for enhancing the catalytic performance or expanding the application area.

Several approaches have been reported for embedding metal NPs in MOF pores that produce excellent catalysts with favorable combinations of metal NPs and MOFs. These techniques include chemical vapor deposition (CVD),[16] solution impregnation,[17] plasma deposition,[18] and solid grinding.[19] Although many new loading methods have been attempted, these methods must be improved to conventionally load the metal precursor into the MOF pores and control the size of small metal NPs without agglomeration. However, impregnating sufficient amounts of metal precursors and/or NPs into the micropores of MOFs is challenging owing to their

Received: February 13, 2024
Revised: April 6, 2024
Accepted: April 12, 2024
Published: April 23, 2024

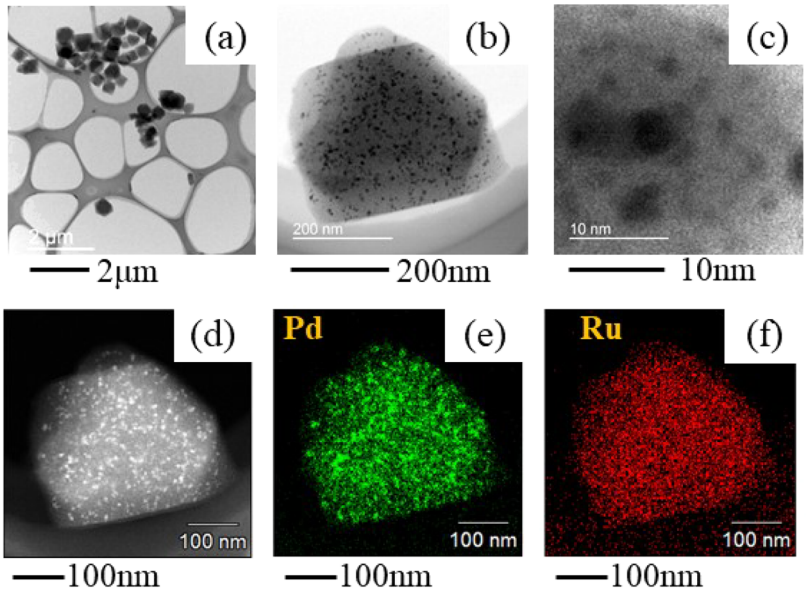

Figure 1. (a)−(c) TEM and (d) HAADF-STEM images of PdRu@MIL-101(Cr), (e) Pd-L STEM-EDX map (green), and (f) Ru-L STEM-EDX map (red) obtained for PdRu NPs immobilized in MIL-101(Cr).

complex pore structure.[17] Impregnation with supercritical carbon dioxide ($scCO_2$) is an effective approach for the uniform decoration and impregnation of porous materials.[20−24] $ScCO_2$-assisted immobilization of metal NPs on porous materials results in high catalytic activity.[25−28] Furthermore, $scCO_2$-based emerging technology allows us to obtain unique and varied morphologies, such as dispersed species, films, and high-surface-area NPs. The morphology of the products could be improved by varying the operating temperature, pressure, contact time, and CO_2 volume rate.[29,30] $ScCO_2$ can surpass the diffusivity and mass transfer limitations of conventional solvents and load sufficient amounts of target materials, such as metal precursors, into the pores and MOF surfaces.[31] Currently, drying with $scCO_2$ is used to improve the pore stabilities of the MOFs.[32−35] Recently, immobilization techniques using catalytically active bimetallic NPs assisted by $scCO_2$ have been considered for the preparation of porous carbon and silica materials.[36−38]

In this study, catalytically active PdRu bimetallic NPs immobilized in the pores and surfaces of MOFs, such as MIL-101(Cr), using an $scCO_2$-assisted immobilization technique is examined. A catalytic CO oxidation reaction was used to evaluate the catalytic performance of the bimetallic PdRu NPs immobilized on MIL-101(Cr). Although Pd and Ru are immiscible at the atomic level in the bulk state,[39] PdRu NPs exhibit higher catalytic activity for CO oxidation than Rh, Pd, and Ru monometallic NPs.[40] A previous study successfully immobilized PdRu NPs in the mesopores of mesoporous SiO_2, and this catalyst exhibited higher catalytic activity during the oxidation of CO.[41] The effective mixing of different metals and the formation of bimetallic PdRu NPs were facilitated in the nanosized mesopores of the MOF, such as MIL-101(Cr). The combination of PdRu NPs with MIL-101(Cr) may significantly enhance the catalytic activity owing to the synergistic effect of the combination of two metals, Pd and Ru, small bimetal particle formation, and charge-transfer interactions between the bimetal NPs and the MOF. The porous structure of MIL-101 (Cr) with a large specific surface area provides a natural space for loading highly dispersed bimetallic NP catalysts without agglomeration. The porous structure of MIL-101(Cr) increased the contact between the substrate and the catalyst, facilitating the reaction.

2. EXPERIMENTAL METHODS

2.1. MIL-101(Cr) Preparation. The methodology for synthesizing MIL-101(Cr) via hydrothermal methods from a suspension comprising $Cr(NO_3)_3{\cdot}9H_2O$, terephthalic acid (TPA), hydrofluoric acid (40%), and H_2O in a molar ratio of 1:1.5:1:280 has been described previously.[23] The suspension was heated for 10 h at 493 K in a Teflon-lined autoclave. Upon cooling, the green MIL-101 (Cr) powder was recovered by filtration, followed by washing with water and ethanol. The resulting MIL-101(Cr) was immersed in a 1 M NH_4F solution at 343 K for 24 h to remove any residual terephthalic acid present within its pores. After washing, the product underwent another filtration process and was dried overnight at 373 K under reduced pressure or via $scCO_2$-assisted drying at 373 K and 20 MPa. The N_2-accessible surface area of MIL-101(Cr) (3400 $m^2{\cdot}g^{-1}$) was determined by using N_2 sorption−desorption experiments (Micrometrics TriStar 3000).

2.2. Immobilization of PdRu NPs on MIL-101(Cr). The details of the immobilization method have been described in a previous study.[41] $Pd(OAc)_2$, $Ru(acac)_3$, and $Rh(OAc)_2$ were used as metal NP precursors. Acetone was used as a cosolvent to enhance the solubility of the metal precursors in $scCO_2$. To synthesize PdRu@MIL-101(Cr), 2.0 g of MIL-101(Cr) and 0.5 g of a mixture containing $Pd(OAc)_2$ and $Ru(acac)_3$ (PdRu precursors) were added to 20 mL of acetone. The mixture was then transferred to a high-pressure cell (200 mL capacity), and CO_2 was introduced into it via a preheater at 20 MPa and 343 K. Then, the cell was immersed in an air bath at 343 K, and the mixture was stirred for 24 h using a magnetic stirrer. After each experiment, the pressure in the cell was gradually released to atmospheric pressure for approximately 30 min before the contents were extracted. The residual acetone was eliminated by centrifugation, and the resulting precipitate was subsequently reduced in a mixed stream of H_2 and N_2 (each at 5 $mL{\cdot}min^{-1}$) at 473 K for 3 h. During the reduction step, the

https://doi.org/10.1021/acsomega.4c01401
ACS Omega 2024, 9, 20437−20443

PdRu NPs were dispersed within the pores and on the surface of MIL-101(Cr).

2.3. Characterization of PdRu@MIL-101(Cr). The structure of PdRu@MIL-101(Cr) was determined using transmission electron microscopy (TEM; H-7100FA, Hitachi, Tokyo, Japan) and high-angle annular dark-field scanning transmission electron microscopy (HAADF-STEM; JEM-ARM200CF, JEOL, Tokyo, Japan). The crystal structures of the samples were confirmed by X-ray diffraction (XRD) using Cu-Ka radiation (XRD-7000L, Shimadzu, Kyoto, Japan). The composition of PdRu embedded in MIL-101(Cr) was determined using energy-dispersive X-ray fluorescence (XRF) spectrometry (SEA1000A, Seiko Instruments Inc., Tokyo, Japan). Quantitative elemental analyses of Pd, Ru, and Cr were also performed. The uncertainty in the composition of PdRu was ±1.2 wt %. The Pd: Ru atomic ratio of PdRu@MIL-101(Cr) was determined using XRF.

2.4. Catalytic Performance of PdRu@MIL-101(Cr). The catalytic performance of PdRu@MIL-101(Cr) was determined by examining the catalyzed CO oxidation reactions. The CO oxidation reactions were conducted in a fixed-bed plug-flow reactor.[41,42] The catalyst (100 mg) was dispersed onto glass sand (30−50 mesh) and introduced into the reactor via stainless steel pipes (inner diameter 15 mm, length 50 mm). Pure CO (1 vol %), O_2 (20 vol %), and He (79 vol %) were individually regulated by mass flow controllers, blended in a mixing chamber, and subsequently passed through the reactor at a flow rate of 100 mL·min^{-1}. Gas chromatography with a TCD detector (GC; GC-2014, Shimadzu, Kyoto, Japan) was used to analyze the reaction products. For catalytic CO oxidation reaction experiments, the CO conversion accuracy was assumed to be within ±2.0%. The reactor maintained a temperature control accuracy of ±0.5 K.

3. RESULTS AND DISCUSSION

3.1. Immobilization of PdRu NPs on MIL-101(Cr) Using $ScCO_2$. The TEM images of PdRu@MIL-101(Cr) are shown in Figure 1a−c. The particle size of MIL-101(Cr) is approximately 400 nm. The surface morphologies of MIL-101(Cr) before and after impregnation with NPs are not significantly different. The TEM images in Figure 1a−c show that $scCO_2$-assisted impregnation facilitates the distribution of PdRu NPs throughout MIL-101(Cr). The EDX spectra of the metal NPs (Figure S1) confirm the presence of Pd−Ru NPs in PdRu@MIL-101(Cr). Small PdRu NPs (2−3 nm) are incorporated into the pores, and larger particles (4−6 nm) are supported on the surface of MIL-101(Cr). The average pore size distribution of MIL-101(Cr) (calculated using the Barrett−oyner−Halenda (BJH) method from the nitrogen sorption isotherm) is 2.0 nm. These pore sizes are likely to accommodate the particle sizes of the small PdRu NPs immobilized inside the pores of MIL-101(Cr) via $scCO_2$-assisted immobilization. The efficient immobilization of the target materials within the pores of MIL-101(Cr) was facilitated by the high diffusivity and low viscosity of $scCO_2$. Additionally, the purposely engineered pore structure and dimensions of MIL-101(Cr) prevented excessive growth of PdRu NPs during the reduction process. By contrast, the large PdRu NPs were partially distributed on the surface of the MIL-101(Cr) particles during reduction. The surface of MIL-101(Cr) stabilized the PdRu NPs through interactions with the carboxylate groups and prevented particle aggregation.

To better investigate the distribution of PdRu on MIL-101(Cr), PdRu@MIL-101(Cr) was examined using HAADF-STEM coupled with EDX, and the obtained elemental maps are shown in Figure 1d−f. Figure 1d shows a HAADF-STEM image of PdRu@MIL-101(Cr), whereas Figure 1e,f shows the Pd-L and Ru-L STEM-EDX mappings, respectively. The PdRu NPs are uniformly distributed on MIL-101(Cr). While Pd and Ru are typically immiscible across the entire composition in the bulk form,[39] their mixing is expedited and enhanced within the nanoscale pores and on the surface of MIL-101(Cr). After the metal precursors were immobilized on the mesopores and surface of MIL-101(Cr) using $scCO_2$, reduction was performed. Microscopic images show that the obtained PdRu NPs were not agglomerated; however, they were randomly and highly dispersed within the cavities and on the surface of MIL-101(Cr).

The XRD patterns of pristine MIL-101(Cr) are shown in Figure 2a; a similar XRD pattern was reported by Horcajada et al.[43] Figure 2b,c shows the XRD patterns of Pd@MIL-101 and Ru@MIL-101(Cr), respectively. The Pd(111) and Ru(100) peaks are observed at 40.1 and 38.3°, respectively. Regarding PdRu@MIL-101(Cr), signals corresponding to Pd and Ru NPs are observed (Figure 2d). The corresponding patterns of the PdRu@MIL-101(Cr) composites are analogous to those of pristine MIL-101(Cr), confirming that the structure remained intact after immobilization. Although XRD is an effective approach for investigating the crystal structures of bimetallic alloy formations, the peak positions of the PdRu NPs did not shift from those of pure Pd or Ru NPs. If the PdRu NPs formed a solid-solution alloy, their diffraction peaks should theoretically be located between the standard peaks of Pd and Ru. The solid-solution PdRu alloy NPs have an XRD pattern comprising two component metals, and the positions of the diffraction peaks vary from those observed for monometallic NPs of Ru or Pd.[40] Metal NPs in MIL-101(Cr) may form Pd−Ru heterojunctions rather than solid-solution PdRu alloys.

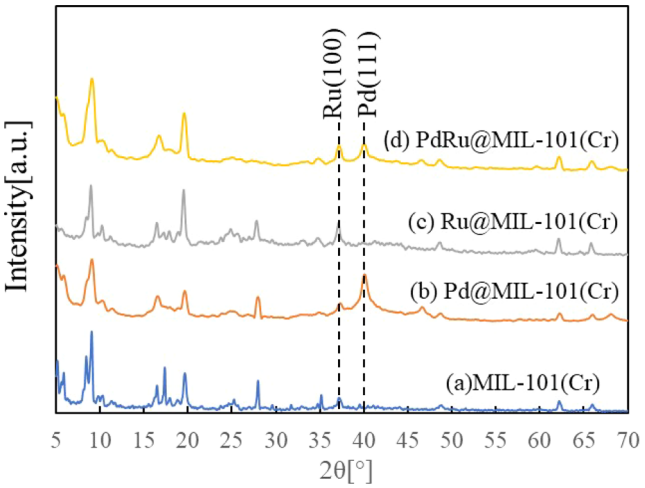

Figure 2. XRD patterns of (a) pristine MIL-101(Cr), (b) Pd@MIL-101(Cr), (c) Ru@MIL-101(Cr), and (d)PdRu@MIL-101(Cr) prepared with $scCO_2$-assisted immobilization.

Figure 3 shows the effect of the ratio of Pd and Ru precursors in the reaction feed on the final PdRu NP composition. The quantity of Pd integrated into the PdRu NPs could be readily increased by increasing the proportion of its precursor, $Pd(OAc)_2$, in the feed mixture, as illustrated in

https://doi.org/10.1021/acsomega.4c01401
ACS Omega 2024, 9, 20437−20443

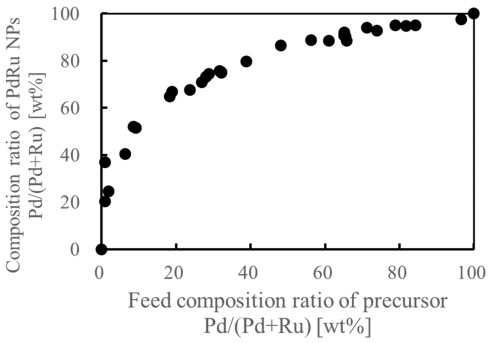

Figure 3. Effect of the precursor composition of Pd and Ru in the reaction feeds on the final composition of PdRu NPs on MIL-101(Cr).

Figure 3. When the amount of $Pd(OAc)_2$ reached approximately 10 wt %, the resulting ratio of Pd in PdRu NPs approached 50 wt %. Similar behavior was observed for porous SiO_2 in a previous study.[41] This suggests that the incorporation of Pd was more favorable than that of Ru, as the precursor of the latter, $Ru(acac)_3$, exhibited higher hydrophobicity and steric bulk than the Pd precursor. This difference in the hydrophobicity and steric bulk between $Ru(acac)_3$ and $Pd(OAc)_2$ is attributed to the differences in their ligands. These factors influence the percolation of the precursors within the nanopores and on the surfaces of the supports, consequently determining the quantity of metal accessible for incorporation into the resulting NPs. The adsorption patterns of the metallic precursors on the support can be correlated with their solubility in the $scCO_2$ solution and their interactions with the support materials, such as MIL-101(Cr). The composition of the PdRu NPs on MIL-101(Cr) can control the feed composition of metal precursors such as $Pd(OAc)_2$ and $Ru(acac)_3$.

3.2. CO Oxidation Catalytic Activity of PdRu@MIL-101(Cr). To investigate the catalytic performance of PdRu@MIL-101(Cr) in the catalytic oxidation of CO, PdRu, Pd, Ru, and Rh NPs were immobilized on MIL-101(Cr) using $scCO_2$-assisted immobilization. A control experiment was conducted by using a mixture of Pd@MIL-101(Cr) and Ru@MIL-101(Cr) as the catalysts. Figure 4 shows the CO conversion percentages achieved using each system. MIL-101(Cr) has been intensively studied for CO adsorbents,[44] and the pristine MIL-101(Cr) shows lower catalytic activity below 200 °C.

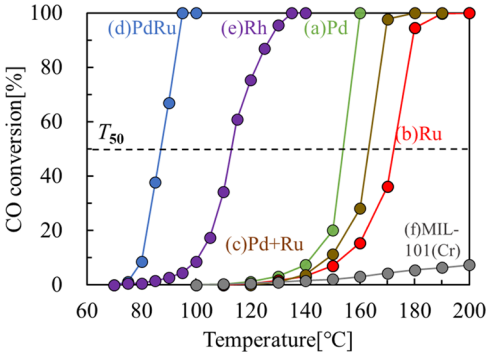

Figure 4. Temperature dependence of the catalytic CO oxidation promoted by (a) Pd (green), (b) Ru (red), (c) Pd + Ru physical mixture (brown), (d) PdRu (blue), and (e) Rh (purple) NPs immobilized on MIL-101(Cr) and (f) pristine MIL-101(Cr) (gray).

PdRu@MIL-101(Cr) exhibited the highest activity for the reaction of CO to CO_2, necessitating a lower temperature (by 65−85 °C) compared to Pd@MIL-101(Cr) and Ru@MIL-101(Cr). Furthermore, the temperature was lower than that of the most expensive precious metal catalyst, Rh NPs; therefore, the CO oxidation efficiency of PdRu@MIL-101(Cr) was higher than that of Rh. The conversion promoted by a physical mixture of Pd@MIL-101(Cr) and Ru@MIL-101(Cr) yielded results that differed from those obtained using PdRu@MIL-101(Cr). The former generally behaved as a Pd@MIL-101(Cr) catalyst because it shielded the effect of Ru@MIL-101(Cr) due to its higher CO oxidation ability. Furthermore, PdRu@MIL-101(Cr) was more efficient in CO oxidation than PdRu@SiO_2.[41] The T_{50} (defined as the temperature at which the reaction from CO to CO_2 reaches 50%) of PdRu@MIL-101(Cr) was 88 °C and that of PdRu@SiO_2 was 142 °C. The T_{50} value of PdRu@MIL-101(Cr) was significantly lower than that of PdRu@SiO_2. The PdRu NPs of PdRu@MIL-101(Cr) were smaller than those of PdRu@SiO_2 because MIL-101(Cr) (surface area of 3400 $m^2 \cdot g^{-1}$; average pore width of 2.0 nm) has a higher surface area and smaller pore size than those of the mesoporous SiO_2 (surface area, 587 $m^2 \cdot g^{-1}$; average pore width, 4.4 nm). The charge-transfer interaction between the PdRu NPs and MIL-101(Cr) may also accelerate the catalytic activity.

Figure 5 shows the effect of the metal composition of PdRu@MIL-101(Cr) on catalytic CO oxidation. The T_{50} values of all of the PdRu@MIL-101 (Cr) samples were lower than those of Pd@MIL-101(Cr) and Ru@MIL-101(Cr), reaching their lowest values when the mass ratio of Pd to Ru in

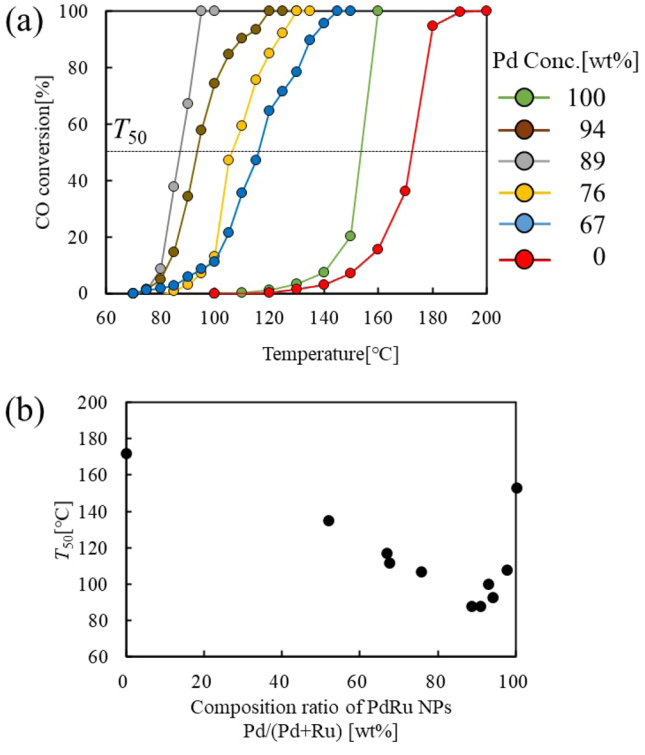

Figure 5. (a) Effect of the metal composition of PdRu NPs on the temperature dependence of the catalytic CO oxidation reaction; (b) relationship between the composition of Pd in PdRu@MIL-101(Cr) and T_{50} (the temperature at which the reaction from CO to CO_2 reaches 50%).

https://doi.org/10.1021/acsomega.4c01401
ACS Omega 2024, 9, 20437−20443

the bimetallic NPs was 89/11. The addition of a small amount of Ru to Pd significantly enhanced its catalytic activity. A comparable inverse volcano-shaped relationship between CO oxidation and Pd content in bimetallic systems has been documented for PdRu solid-solution alloy NPs.[40]

The improvement in the catalytic activity of PdRu@MIL-101(Cr) likely stemmed from the creation of a novel electronic state introduced by the nanoscale mixing of Pd and Ru in mesopores and on the surface of MIL-101(Cr). PdRu bimetallic NPs exhibit an electronic structure similar to that of Rh because Rh is located between Ru and Pd in the periodic table.[45]

Furthermore, we confirmed the stability of PdRu@MIL-101(Cr) during the CO oxidation. Figure 6 compares the

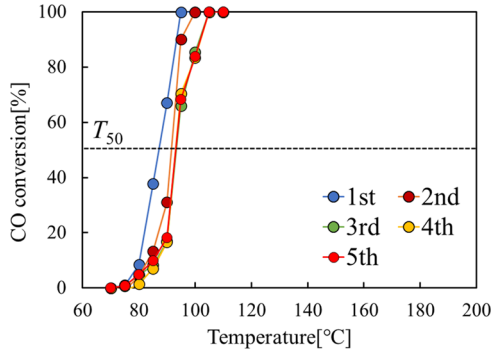

Figure 6. Cyclic test was used to study the temperature dependence of catalytic CO oxidation promoted by PdRu NPs immobilized on MIL-101(Cr).

initial CO oxidation catalytic activity after five cycles. The catalytic activity of PdRu@MIL-101(Cr) decreased slightly with an increase in the number of cycles in the catalyzed CO oxidation test. PdRu@MIL-101(Cr) exhibited high catalytic performance and high durability in the catalytic CO oxidation reaction.

3.3. Intermolecular Interaction between PdRu and MIL-101(Cr). The interactions between MIL-101(Cr) and PdRu NPs were investigated by using X-ray photoelectron spectroscopy (XPS). The Pd 3d spectrum of PdRu@MIL-101(Cr) is shown in Figure 7. The peak binding energies at 335.2 eV ($3d_{5/2}$) and 340.5 eV ($3d_{3/2}$) confirmed the presence of Pd^0. The peak at 337.1 eV suggests that a Pd−O component (Pd^{2+}) was present, possibly resulting from the bond between the carboxylate groups of TPA and Pd.

The coordination of the carboxylate groups of TPA to Pd may have been induced by its electron-donating abilities. Interactions between the metal (M) NPs and MIL-101(Cr) occurred via M−O bonds, leading to charge-transfer interactions between the metal NPs and MIL-101(Cr). This may have contributed to the enhanced catalytic activity of PdRu@MIL-101(Cr). The synergistic effect of PdRu@MIL-101(Cr) enhanced its catalytic activity. Additionally, these effects may be attributed to the combination of the two metals (Pd and Ru), the formation of small metal particles on the pores and surface of MIL-101(Cr), and the charge-transfer interactions between the metal NPs and MIL-101(Cr).

4. CONCLUSIONS

The $scCO_2$-assisted immobilization of bimetallic NPs on the MOFs was successfully achieved. Impregnation with $scCO_2$ is

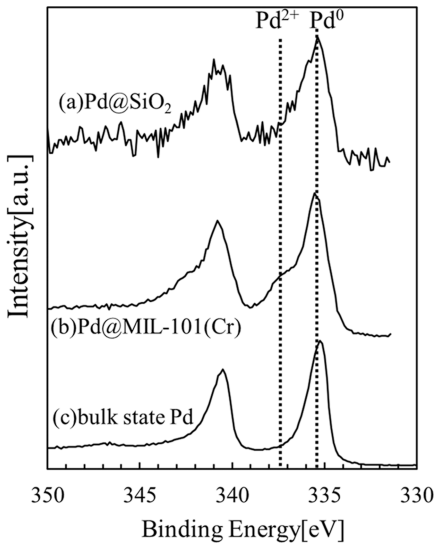

Figure 7. XPS spectra of (a) Pd@SiO_2, (b) Pd@MIL-101(Cr), and (c) bulk state Pd.

an effective approach for forming bimetallic NPs on MOFs. The resulting PdRu@MIL-101(Cr) catalyst exhibited enhanced CO oxidation. The nanosized mesopores and surfaces of the MOF facilitate the effective mixing of different metals and the formation of bimetallic NPs. The formation of bimetallic NPs on the MOF resulted in a significant synergistic effect for the enhancement of catalytic reactions such as CO oxidation. The synergistic effects are based on the combination of the two metals, the formation of small metal NPs on the pores and surface of the MOF, and the charge-transfer interactions between the metal NPs and the MOF. These synergistic effects could not be achieved using MOFs or metal NPs alone. The bimetallic NP/MOF composites may open new avenues for the design of catalytically active nanomaterial catalysts by improving the performance of existing MOFs.

■ ASSOCIATED CONTENT

Supporting Information

The Supporting Information is available free of charge at https://pubs.acs.org/doi/10.1021/acsomega.4c01401.

The EDX spectra of Pd−Ru NPs for PdRu@MIL-101(Cr) (PDF)

■ AUTHOR INFORMATION

Corresponding Author

Kiyoshi Matsuyama − *Department of Life, Environment and Applied Chemistry, Fukuoka Institute of Technology, Fukuoka 811-0295, Japan*; orcid.org/0000-0002-9037-4908; Email: matsuyama@fit.ac.jp

Authors

Takumi Matsuoka − *Department of Life, Environment and Applied Chemistry, Fukuoka Institute of Technology, Fukuoka 811-0295, Japan*

Masashi Eiro − *Department of Life, Environment and Applied Chemistry, Fukuoka Institute of Technology, Fukuoka 811-0295, Japan*

Takafumi Kato − *Department of Chemical Engineering, Fukuoka University, Fukuoka 814-0180, Japan*

https://doi.org/10.1021/acsomega.4c01401
ACS Omega 2024, 9, 20437−20443

Tetsuya Okuyama − *Department of Collaborative Interdisciplinary Engineering Sciences, Kyushu University, Kasuga 816-8580, Japan*

Complete contact information is available at: https://pubs.acs.org/10.1021/acsomega.4c01401

Notes

The authors declare no competing financial interest.

■ ACKNOWLEDGMENTS

This study was partially supported by the JSPS KAKENHI (grant number JP24K08153) and the Iketani Science and Technology Foundation (grant number 0351187-A). The authors would like to thank Editage (www.editage.jp) for English language editing.

■ REFERENCES

(1) Daglar, H.; Gulbalkan, H. C.; Avci, G.; Aksu, G. O.; Altundal, O. F.; Altintas, C.; Erucar, I.; Keskin, S. Effect of Metal−Organic Framework (MOF) Database Aelection on the Assessment of Gas Storage and Separation Potentials of Mofs. *Angew. Chem., Int. Ed.* **2021**, *60* (14), 7828−7837.

(2) Knebel, A.; Caro, J. Metal−Organic Frameworks and Covalent Organic Frameworks as Disruptive Membrane Materials for Energy-Efficient Gas Separation. *Nat. Nanotechnol.* **2022**, *17* (9), 911−923.

(3) Liu, Y.; Wu, J.; Li, W.; Li, J.; Han, H.; Song, Z. Responsive Metal−Organic Framework Nanocarrier Delivery System: An Effective Solution against Bacterial Infection. *Coord. Chem. Rev.* **2023**, *496*, No. 215431.

(4) Wang, Q.; Astruc, D. State of the Art and Prospects in Metal−Organic Framework (MOF)-Based and Mof-Derived Nanocatalysis. *Chem. Rev.* **2020**, *120* (2), 1438−1511.

(5) Wang, Q.; Yang, G.; Fu, Y.; Li, N.; Hao, D.; Ma, S. Nanospace Engineering of Metal-Organic Frameworks for Heterogeneous Catalysis. *ChemNanoMat* **2022**, *8* (1), No. e202100396.

(6) Tsumori, N.; Chen, L.; Wang, Q.; Zhu, Q.-L.; Kitta, M.; Xu, Q. Quasi-Mof: Exposing Inorganic Nodes to Guest Metal Nanoparticles for Drastically Enhanced Catalytic Activity. *Chem.* **2018**, *4* (4), 845−856.

(7) Yang, Q.; Xu, Q.; Jiang, H.-L. Metal−Organic Frameworks Meet Metal Nanoparticles: Synergistic Effect for Enhanced Catalysis. *Chem. Soc. Rev.* **2017**, *46* (15), 4774−4808.

(8) Mukoyoshi, M.; Kitagawa, H. Nanoparticle/Metal−Organic Framework Hybrid Catalysts: Elucidating the Role of the Mof. *Chem. Commun.* **2022**, *58* (77), 10757−10767.

(9) Yoshimaru, S.; Sadakiyo, M.; Staykov, A.; Kato, K.; Yamauchi, M. Modulation of the Catalytic Activity of Pt Nanoparticles through Charge-Transfer Interactions with Metal−Organic Frameworks. *Chem. Commun.* **2017**, *53* (50), 6720−6723.

(10) Liu, L.; Corma, A. Bimetallic Sites for Catalysis: From Binuclear Metal Sites to Bimetallic Nanoclusters and Nanoparticles. *Chem. Rev.* **2023**, *123* (8), 4855−4933.

(11) Yao, Y.; Dong, Q.; Brozena, A.; Luo, J.; Miao, J.; Chi, M.; Wang, C.; Kevrekidis, I. G.; Ren, Z. J.; Greeley, J.; Wang, G.; Anapolsky, A.; Hu, L. High-Entropy Nanoparticles: Synthesis-Structure-Property Relationships and Data-Driven Discovery. *Science* **2022**, *376* (6589), No. eabn3103.

(12) Kusada, K.; Wu, D.; Kitagawa, H. New Aspects of Platinum Group Metal-Based Solid-Solution Alloy Nanoparticles: Binary to High-Entropy Alloys. *Chem.—Eur. J.* **2020**, *26* (23), 5105−5130.

(13) Duan, M.; Jiang, L.; Zeng, G.; Wang, D.; Tang, W.; Liang, J.; Wang, H.; He, D.; Liu, Z.; Tang, L. Bimetallic Nanoparticles/Metal-Organic Frameworks: Synthesis, Applications and Challenges. *Appl. Mater. Today* **2020**, *19*, No. 100564.

(14) El-Shall, M. S.; Abdelsayed, V.; Khder, A. E. R. S.; Hassan, H. M. A.; El-Kaderi, H. M.; Reich, T. E. Metallic and Bimetallic Nanocatalysts Incorporated into Highly Porous Coordination Polymer Mil-101. *J. Mater. Chem.* **2009**, *19* (41), 7625−7631.

(15) Rösler, C.; Dissegna, S.; Rechac, V. L.; Kauer, M.; Guo, P.; Turner, S.; Ollegott, K.; Kobayashi, H.; Yamamoto, T.; Peeters, D.; Wang, Y.; Matsumura, S.; Van Tendeloo, G.; Kitagawa, H.; Muhler, M.; Llabrés i Xamena, F. X.; Fischer, R. A. Encapsulation of Bimetallic Metal Nanoparticles into Robust Zirconium-Based Metal−Organic Frameworks: Evaluation of the Catalytic Potential for Size-Selective Hydrogenation. *Chem.—Eur. J.* **2017**, *23* (15), 3583−3594.

(16) Zhang, M.; Guan, J.; Zhang, B.; Su, D.; Williams, C. T.; Liang, C. Chemical Vapor Deposition of $Pd(C_3H_5)(C_5H_5)$ to Synthesize Pd@MOF-5 Catalysts for Suzuki Coupling Reaction. *Catal. Lett.* **2012**, *142* (3), 313−318.

(17) Aijaz, A.; Karkamkar, A.; Choi, Y. J.; Tsumori, N.; Rönnebro, E.; Autrey, T.; Shioyama, H.; Xu, Q. Immobilizing Highly Catalytically Active Pt Nanoparticles inside the Pores of Metal−Organic Framework: A Double Solvents Approach. *J. Am. Chem. Soc.* **2012**, *134* (34), 13926−13929.

(18) Sadakiyo, M.; Yoshimaru, S.; Kasai, H.; Kato, K.; Takata, M.; Yamauchi, M. A New Approach for the Facile Preparation of Metal−Organic Framework Composites Directly Contacting with Metal Nanoparticles through Arc Plasma Deposition. *Chem. Commun.* **2016**, *52* (54), 8385−8388.

(19) Jiang, H.-L.; Liu, B.; Akita, T.; Haruta, M.; Sakurai, H.; Xu, Q. Au@ZIF-8: CO Oxidation over Gold Nanoparticles Deposited to Metal−Organic Framework. *J. Am. Chem. Soc.* **2009**, *131* (32), 11302−11303.

(20) Zhang, F.; Zhang, B.; Feng, J.; Tan, X.; Liu, L.; Liu, L.; Han, B.; Zheng, L.; Zhang, J.; Tai, J.; Zhang, J. Highly Mesoporous Ru-Mil-125-NH_2 Produced by Supercritical Fluid for Efficient Photocatalytic Hydrogen Production. *ACS Appl. Energy Mater.* **2019**, *2* (7), 4964−4970.

(21) Zhao, Y.; Zhang, J.; Song, J.; Li, J.; Liu, J.; Wu, T.; Zhang, P.; Han, B. Ru Nanoparticles Immobilized on Metal−Organic Framework Nanorods by Supercritical CO_2-Methanol Solution: Highly Efficient Catalyst. *Green Chem.* **2011**, *13* (8), 2078−2082.

(22) Türk, M.; Erkey, C. Synthesis of Supported Nanoparticles in Supercritical Fluids by Supercritical Fluid Reactive Deposition: Current State, Further Perspectives and Needs. *J. Supercrit. Fluids* **2018**, *134*, 176−183.

(23) Matsuyama, K.; Motomura, M.; Kato, T.; Okuyama, T.; Muto, H. Catalytically Active Pt Nanoparticles Immobilized inside the Pores of Metal Organic Framework Using Supercritical CO_2 Solutions. *Microporous Mesoporous Mater.* **2016**, *225*, 26−32.

(24) Siril, P. F.; Türk, M. Synthesis of Metal Nanostructures Using Supercritical Carbon Dioxide: A Green and Upscalable Process. *Small* **2020**, *16* (49), No. 2001972.

(25) Matsuyama, K.; Tanaka, S.; Kato, T.; Okuyama, T.; Muto, H.; Miyamoto, R.; Bai, H.-z. Supercritical Fluid-Assisted Immobilization of Pd Nanoparticles in the Mesopores of Hierarchical Porous SiO_2 for Catalytic Applications. *J. Supercrit. Fluids* **2017**, *130*, 140−146.

(26) Ashikari, Y.; Maekawa, K.; Ishibashi, M.; Fujita, C.; Shiosaki, K.; Bai, H.; Matsuyama, K.; Nagaki, A. Stille, Heck, and Sonogashira Coupling and Hydrogenation Catalyzed by Porous-Silica-Gel-Supported Palladium in Batch and Flow. *Green Process. Synth.* **2021**, *10* (1), 722−728.

(27) Ashikari, Y.; Maekawa, K.; Takumi, M.; Tomiyasu, N.; Fujita, C.; Matsuyama, K.; Miyamoto, R.; Bai, H.; Nagaki, A. Flow Grams-Per-Hour Production Enabled by Hierarchical Bimodal Porous Silica Gel Supported Palladium Column Reactor Having Low Pressure Drop. *Catal. Today* **2022**, *388*−*389*, 231−236.

(28) Yamada, T.; Ogawa, A.; Masuda, H.; Teranishi, W.; Fujii, A.; Park, K.; Ashikari, Y.; Tomiyasu, N.; Ichikawa, T.; Miyamoto, R.; Bai, H.; Matsuyama, K.; Nagaki, A.; Sajiki, H. Pd Catalysts Supported on Dual-Pore Monolithic Silica Beads for Chemoselective Hydrogenation under Batch and Flow Reaction Conditions. *Catal. Sci. Technol.* **2020**, *10* (18), 6359−6367.

(29) Costa, J. M.; Almeida Neto, A. F. d. Nanocatalysts Deposition Assisted by Supercritical Carbon Dioxide Technology: A Review. *Synth. Met.* **2021**, *271*, No. 116627.
(30) Yousefzadeh, H.; Akgün, I. S.; Barim, S. B.; Sari, T. B.; Eris, G.; Uzunlar, E.; Bozbag, S. E.; Erkey, C. Supercritical Fluid Reactive Deposition: A Process Intensification Technique for Synthesis of Nanostructured Materials. *Chem. Eng. Process.* **2022**, *176*, No. 108934.
(31) Matsuyama, K.; Hayashi, N.; Yokomizo, M.; Kato, T.; Ohara, K.; Okuyama, T. Supercritical Carbon Dioxide-Assisted Drug Loading and Release from Biocompatible Porous Metal-Organic Frameworks. *J. Mater. Chem. B* **2014**, *2* (43), 7551−7558.
(32) Zhang, X.; Chen, Z.; Liu, X.; Hanna, S. L.; Wang, X.; Taheri-Ledari, R.; Maleki, A.; Li, P.; Farha, O. K. A Historical Overview of the Activation and Porosity of Metal−Organic Frameworks. *Chem. Soc. Rev.* **2020**, *49* (20), 7406−7427.
(33) Matsuyama, K. Supercritical Fluid Processing for Metal−Organic Frameworks, Porous Coordination Polymers, and Covalent Organic Frameworks. *J. Supercrit. Fluids* **2018**, *134*, 197−203.
(34) Ushiki, I.; Matsuyama, K.; Smith, R. L. Chapter 15 - Sustainable Approaches for Materials Engineering with Supercritical Carbon Dioxide. In *Sustainable Nanoscale Engineering*; Szekely, G.; Livingston, A., Eds.; Elsevier, 2020; pp 395−414.
(35) Matsuyama, K.; Kawahara, Y.; Shoji, A.; Kato, T.; Okuyama, T. Supercritical CO_2-Assisted Formation of Metal−Organic Framework-Loaded Porous Polystyrene Membranes for Dye Removal. *J. Appl. Polym. Sci.* **2023**, *140* (35), No. e54347.
(36) Barim, S. B.; Bozbag, S. E.; Yu, H.; Kızılel, R.; Aindow, M.; Erkey, C. Mesoporous Carbon Aerogel Supported Ptcu Bimetallic Nanoparticles Via Supercritical Deposition and Their Dealloying and Electrocatalytic Behaviour. *Catal. Today* **2018**, *310*, 166−175.
(37) Qiao, Y.; Said, N.; Rauser, M.; Yan, K.; Qin, F.; Theyssen, N.; Leitner, W. Preparation of SBA-15 Supported Pt/Pd Bimetallic Catalysts Using Supercritical Fluid Reactive Deposition: How Do Solvent Effects During Material Synthesis Affect Catalytic Properties? *Green Chem.* **2017**, *19* (4), 977−986.
(38) Sánchez-Miguel, E.; Tenorio, M. J.; Morère, J.; Cabañas, A. Green Preparation of Ptru and Ptcu/Sba-15 Catalysts Using Supercritical CO_2. *J. CO_2 Util.* **2017**, *22*, 382−391.
(39) Tripathi, S. N.; Bharadwaj, S. R.; Dharwadkar, S. R. The Pd-Ru System (Palladium-Ruthenium). *J. Phase Equilib.* **1993**, *14* (5), 638−642.
(40) Kusada, K.; Kobayashi, H.; Ikeda, R.; Kubota, Y.; Takata, M.; Toh, S.; Yamamoto, T.; Matsumura, S.; Sumi, N.; Sato, K.; Nagaoka, K.; Kitagawa, H. Solid Solution Alloy Nanoparticles of Immiscible Pd and Ru Elements Neighboring on Rh: Changeover of the Thermodynamic Behavior for Hydrogen Storage and Enhanced CO-Oxidizing Ability. *J. Am. Chem. Soc.* **2014**, *136* (5), 1864−1871.
(41) Matsuyama, K.; Tomiyasu, N.; Inoue, K.; Yokomizo, R.; Okuyama, T.; Muto, H. Catalytically Active Pdru and Curu Bimetallic Nanoparticle Formation in the Mesoporous Sio_2 by Supercritical CO_2-Assisted Immobilization. *J. Supercrit. Fluids* **2020**, *160*, No. 104818.
(42) Matsuyama, K.; Tsubaki, T.; Kato, T.; Okuyama, T.; Muto, H. Preparation of Catalytically Active Au Nanoparticles by Sputter Deposition and Their Encapsulation in Metal-Organic Framework of $Cu_3(BTC)_2$. *Mater. Lett.* **2020**, *261*, No. 127124.
(43) Horcajada, P.; Serre, C.; Vallet-Regí, M.; Sebban, M.; Taulelle, F.; Férey, G. Metal−Organic Frameworks as Efficient Materials for Drug Delivery. *Angew. Chem., Int. Ed.* **2006**, *45* (36), 5974−5978.
(44) Vo, T. K.; Kim, J.-H.; Kwon, H. T.; Kim, J. Cost-Effective and Eco-Friendly Synthesis of MIL-101(Cr) from Waste Hexavalent Chromium and Its Application for Carbon Monoxide Separation. *J. Ind. Eng. Chem.* **2019**, *80*, 345−351.
(45) Kobayashi, H.; Kusada, K.; Kitagawa, H. Creation of Novel Solid-Solution Alloy Nanoparticles on the Basis of Density-of-States Engineering by Interelement Fusion. *Acc. Chem. Res.* **2015**, *48* (6), 1551−1559.

https://doi.org/10.1021/acsomega.4c01401
ACS Omega 2024, 9, 20437−20443